Int. J. Electrochem. Sci., 17 **(2022)** Article Number: 221131, doi: 10.20964/2022.11.24

International Journal of
ELECTROCHEMICAL
SCIENCE
www.electrochemsci.org

Nitrogen-doped graphene oxide/carbon nanotubes nanocomposite (N-doped GO/CNTs) as a sensitive electrochemical sensor for detection of oxymetholone in blood serum

Youmin Liu[1], *Chunzheng Peng*[2,*], *Hong Cun Liu*[2], *Huan Ji*[2], *Zheng Wang*[3]

[1] Shanxi Conservancy Technical Iinstitute； Yuncheng 044000,China
[2] School of Physical Education, Changzhou University, Changzhou, 213164, China
[3] Zhongwu Material Research Institute, Changzhou, 213164, China
[*]E-mail: pengchzheng@sina.com

Received: 8 August 2022 / *Accepted:* 8 September 2022 / *Published:* 10 October 2022

In the current study, it has been shown how to make an electrochemical sensor for measuring the amount of oxymetholone in blood serum samples from bikers using a nitrgen-doped graphene oxide and carbon nanotube nanocomposite (N-doped GO/CNTs). The N-doped GO/CNT nanocomposite was created using the pyrolysis technique, and the GCE was modified by electrochemical deposition. N-doped GO/CNT nanocomposite structural studies employing XRD and SEM analysis revealed that the nanocomposite's corrugated sheet-like shape featured GO nanosheets with CNTs scattered on the nanosheets. The EDX elemental analysis revealed that the N atoms in the GO/CNT structure had been successfully doped. According to electrochemical tests using the DPV approach, the detection limit was established as 0.01 ng/mL, the calibration curve demonstrated a linear relationship to the concentration of oxymetholone from 0 to 114 ng/mL, and the sensitivity was attained at 0.18849 μA/ng.mL^{-1}. The linear range and detection limit of the oxymetholone sensor in this work are enhanced and are better than in previous electrochemical reports, according to a comparison of the performance of the electrochemical sensor used in this study and other recently published oxymetholone sensors. Five hours following the race, genuine blood serum samples from four riders were used to test the accuracy and usefulness of N-doped GO/CNTs/GCE for the detection of oxymetholone M. The results showed that the RSD values (3.69% to 4.34%) were appropriate and acceptable for practical analyses in blood serum and clinical samples that were valid and accurate.

Keywords: Nitrogen doping; CNTs, graphene oxide; Nanocomposite; Pyrolysis synthesis; Electrodeposition; oxymetholone ; Differential pulse voltammetry

1. INTRODUCTION

Oxymetholone ($C_{21}H_{32}O_3$) is an anabolic steroid and a 3-oxo-5α- steroid with androgenic activity that is 4,5α-dihydrotestosterone which is substituted by a hydroxymethylidene group at position 2 and by a methyl group at the 17α-position [1-3]. Oxymetholone binds to the androgen receptor with a low affinity but strongly activates androgen receptor-mediated signaling, which increases erythropoietin and protein synthesis [4-6]. Certain kinds of anemia, such as aplastic anemia, myelofibrosis, or hypoplastic anemia brought on by chemotherapy, are treated with oxymetholone [7-9]. The hormone (erythropoietin) involved in the synthesis of red blood cells is increased in quantity as a result of its action [10, 11]. One of the most effective steroids ever created for muscle growth, oxymetholone primarily increases protein synthesis. As a result, bodybuilders and athletes frequently use it [12-14].

Long-term usage of oxymetholone can result in liver tumors or blood-filled cysts in the liver or spleen [15-17]. Oxymetholone is a forbidden anabolic agent included on the WADA Prohibited List. Other negative effects of oxymetholone include nausea, upper stomach pain, and quick weight gain, particularly in the face and middle [18-20]. As a result, determining oxymetholone levels in an athlete's biological samples is crucial. Several studies have been done employing spectrophotometry [21], gas chromatography–mass spectrometry (GC-MS) [22], high-performance liquid chromatography (HPLC) [23], and electrochemical sensor [24] to do this. However, in order to improve the selectivity and sensitivity of oxymetholone sensors' performance, these studies are relatively restricted, and the sensors need to be modified with appropriate nanostructure and nanocomosites with a large surface area-volume ratio [25-29]. In order to determine the amount of oxymetholone in samples of blood serum from cyclists, the fabrication of an electrochemical sensor based on an N-doped GO/CNT nanocomposite has been presented in this study.

2. EXPERIMENT

2.1. Synthesis of nitrogen-doped graphene oxide/carbon nanotubes nanocomposite

The pyrolysis method was used for the synthesis of an N-doped GO/CNTs nanocomposite [30]. 50 ml of 1 g/1 GO (98%, Xiamen Tob New Energy Technology Co., Ltd., China) and 50 ml of 0.5 g/1 CNTs (99%, Guangzhou Hongwu Material Technology Co., Ltd., China) were ultrasonically mixed for 90 minutes. The mixture was then ultrasonically mixed with 1 g of 99 percent urea (Sigma-Aldrich) and 0.5 mg of lignosulfonate (Sigma-Aldrich). The mixture was then dried at 50 °C in a vacuum oven. The mixture was then pyrolyzed in a flowing nitrogen environment for 120 minutes at 750 °C and 5 C/min heating rates. The resultant N-doped GO/CNTs nanocomposite was employed for electrochemical deposition to modify the GCE after cooling [31]. Prior to the electrochemical deposition, the GCE surface (3 mm in diameter) was successively polished with Al_2O_3 slurry powder (0.3 μm, 99.99%, Sigma-Aldrich) on a buff for 15 minutes to reach the mirror-smooth surface. Then, the GCE was ultrasonically rinsed with deionized water and sonicated in 1 mM HNO_3 (99.5%, Sigma-

Aldrich) for 5 minutes followed by sonication in a mixture of water and ethanol (99%, Merck, Germany) in an equal volume ratio for 5 minutes. For electrodeposition, 10.0 mg N-doped GO/CNTs nanocomposite were dispersed in 30 mL of 0.1 M KCl (≥99.0%, Sigma-Aldrich) solution. The electrochemical cell contained a Pt plate as the counter electrode, a GCE as the working electrode, and Ag/AgCl (3 M KCl) as the reference and counter electrodes, respectively. The electrodeposition was carried out using an electrochemical workstation potentiostat (CS1005, Zhengzhou CY Scientific Instrument Co., Ltd., China). The N-doped GO/CNT nanocomposite electrodeposition was carried out at 1.5 V for 4 minutes. The electrode was then thoroughly cleaned with deionized water. In order to serve as a point of comparison, graphene oxide/carbon nanotubes nanocomposite modified GCE (GO/CNTs/GCE) was made using the same process using a combination of GO and CNTs. GO/GCE and CNTs/GCE were made using the same electrodeposition process from dispersed 10.0 mg GO in 30 mL of 0.1 M KCl solution and dispersed 10.0 mg CNTs in 30 mL of 0.1 M KCl solution, respectively.

2.2. Characterizations

For structural and morphological analyses of electrodeposited nanostructures, respectively, scanning electron microscopy (SEM; S4800, Hitachi, Japan) and X-ray diffractometer (XRD; D8 Advance, Bruker-AXS) at 40 KV and 40 mA with a Cu-K X-ray source were used. Through the use of energy-dispersive X-ray spectroscopy, the elemental composition was identified. Differential pulse voltammetry (DPV) technique was used for electrochemical studies which were conducted on an electrochemical workstation potentiostat (CS1005, Zhengzhou CY Scientific Instrument Co., Ltd., China) in 0.1 M phosphate buffer solution (PBS) with pH =7.4 which contained an mixture of equal volume ratio of 0.1M NaH_2PO_4 (99%, Sigma-Aldrich) and 0.1M Na_2HPO_4 (99%).

2.3. Analysis of real sample

Following administration of Anadrol 50 (Samson Pharma, UK), which contains 50 mg of oxymetholone per pill, four cyclists, ages 19 to 25, provided blood samples (sample of 19 years old as name C1, 22 years old as name C2, 23 years old as name C3 and 25 years old as name C4). Due to the short half-life of Anadrol 50—only 16 hours—blood samples were taken after 8 hours of Anadrol administration and centrifuged for 12 minutes at 1500 rpm. The obtained supernatants were filtered before being used to create actual electrochemical study samples of 0.1 M PBS pH 7.4. The conventional standard method was also used in the study of an actual sample.

3. RESULTS AND DISCUSSION

3.1. Structural studies of electrodeposited nanstructures

The SEM images of the electrodeposited GO on GCE and N-doped GO/CNT nanocomposite on GCE are shown in Figure 1. Figure 1a's GO SEM micrograph shows a structure of folded and

wrinkled GO nanosheets that overlap. Figure 1b shows the corrugate-like shape of a nanocomposite made of GO nanosheets with CNTs scattered throughout on GCE. CNTs have a 15 nm diameter on average. The GO/CNTs and N-doped GO/CNTs nanocomposites were electrodeposited on GCE without tangling of CNTs or re-stacking of GO nanosheets. CNTs can act as a nano-spacer between GO nanosheets, essentially preventing GO nanosheet stacking [32-34]. The electrodeposited GO nanosheets and CNTs have a large surface area and numerous pores that can be regarded as nanoporous surfaces that help with diffusion and electron transfer in electrochemical reactions [35-37].

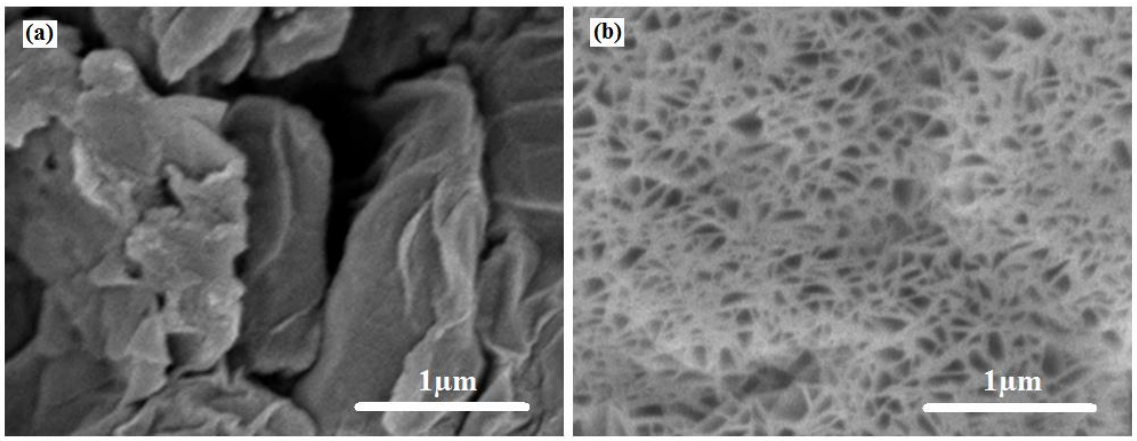

Figure 1. SEM micrographs of (a) GO/GCE, (b) N-doped GO/CNTs/GCE

Figure 2 illustrates the XRD patterns of powder electrodeposited GO, CNTs, GO/CNTs, and N-doped GO/CNT nanocomposite. With an interlayer spacing of 0.83 nm and a distinctive diffraction peak at 10.41° ascribed to the GO's graphitic structure's (001) plane, the XRD pattern of GO shows the synthesis of oxygen functionalities in the graphite's basal plane [38-40]. The graphitic carbon in CNTs with the plane of (002) is depicted by a prominent diffraction peak at 25.69° in the XRD pattern of CNTs [41-43]. The successful electrodeposition of CNTs on the surface of GO nanosheets was shown by the XRD patterns of powder electrodeposited GO/CNTs and N-doped GO/CNTs nanocomposite, which exhibit the two diffraction peaks at 10.40° and 25.70° [44-46]. This was further confirmed by the SEM micrograph, which is shown in Figure 1c. The identical XRD pattern of powdered N-doped GO/CNTs and GO/CNTs suggests that nitrogen doping does not alter the structure of CNTs and the lattice of grapheme [47-49]. The diffraction peak strength in the XRD pattern of N-doped GO/CNTs is, however, somewhat reduced.

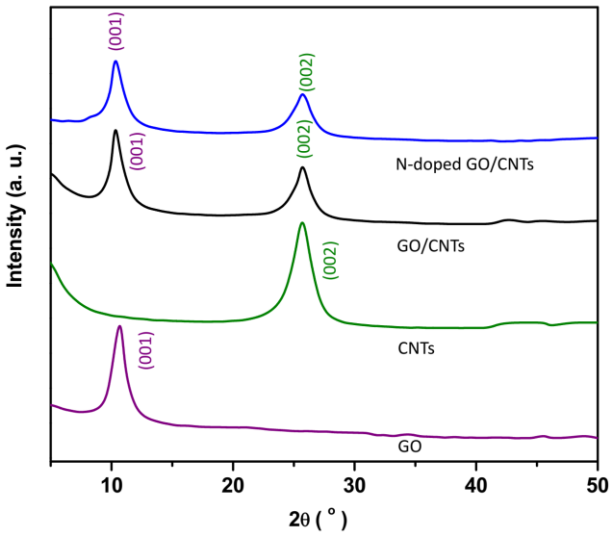

Figure 2. The XRD patterns of powder electrodeposited GO, CNTs, GO/CNTs and N-doped GO/CNTs nanocomposite.

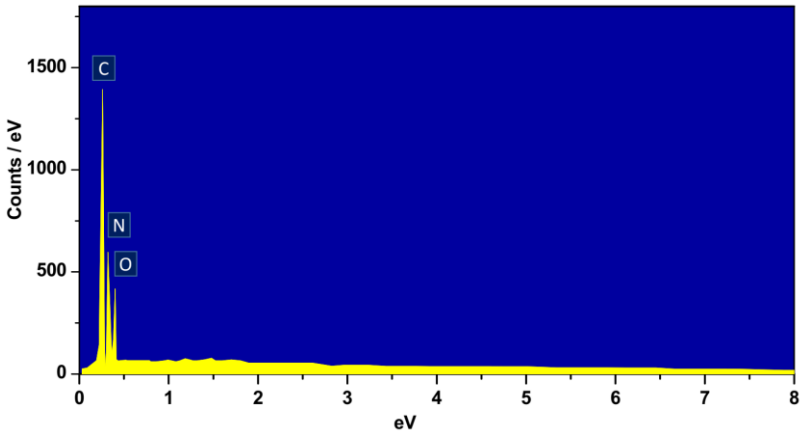

Figure 3. EDX pattern of the N-doped GO/CNTs nanocomposite.

The elemental analysis of the electrodeposited N-doped nanocomposite is shown in Figure 3 using the EDX pattern of the N-doped GO/CNTs. As can be seen, the EDX pattern of the N-doped GO/CNTs contains the three elements C, O, and N. The GO and CNTs are responsible for the nanocomposite's strong carbon peak. The N atoms in the GO/CNT structure were successfully doped, as indicated by the N peak that was found in the EDX pattern [50-52].

3.2. Electrochemical studies

In 0.1M PBS containing 60 ng/mL oxymetholone, Figure 4 displays the DPV curves of the bare GCE, GO/GCE, CNTs/GCE, GO/CNTs/GCE, and N-doped GO/CNTs/GCE in the potential window of 0.30 V to 0.85 V. As can be seen, all electrodes have a distinct peak in the DPV curves. At 0.56 V, 0.56 V, 0.55 V, 0.55 V, and 0.54 V, respectively, the oxidation peaks GCE, GO/GCE, CNTs/GCE, GO/CNTs/GCE, and N-doped GO/CNTs/GCE, which are related to the oxymetholone oxidation steps placed on the A-ring with a two electron oxidation process, are seen. This mechanism may be

associated with the fact that the A-ring contains an appropriate oxidation position to create a conjugated double bond [24, 53, 54]. The peak current of N-doped GO/CNTs/GCE is much greater at a lower potential of 0.54 V than that of GO/GCE, CNTs /GCE, and GO/CNTs/GCE, as shown by GCE's incredibly weak peak and other DPV curves. GO because the large surface area of the 2D sp^2-hybridized carbon nanosheets showed a strong electrical conductivity [55-57]. Doping nitrogen into GO frameworks with substituent heteroatoms can effectively modulate the electronic characteristics, surface and local chemical features of GO [58-60]. The addition of CNTs, which act as conductive linkers and spacers between individual GO nanosheets, results in substantially increased porosity and improved electrical conductivity in GO/CNTs and N-doped GO/CNTs nanocomposites compared to pure GO and CNTs [61-63]. Therefore, the channels generated by the CNTs spacer can be beneficial for the electrolyte ion transfer [64-66]. High porosity in nanocomposites significantly increases specific surface area and improves the kinetics of ionic and electronic transfer [67, 68]. Additionally, by adding nitrogen to nanocomposite materials, it can reduce the diffusion resistance of electrolyte ions in the electrode and give short transit lengths for mass and charge, which can increase electron mobility [69-71]. As a result, N-doped GO/CNTs/GCE was used in the following electrochemical studies for OM sensing.

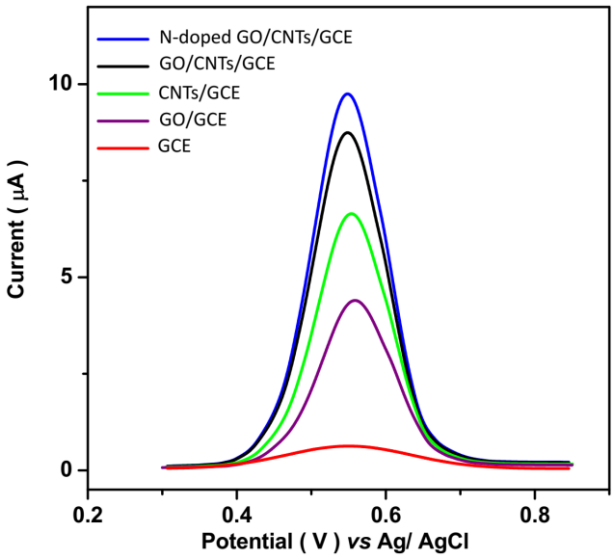

Figure 4. DPV curves of the bare GCE, GO/GCE, CNTs/GCE, GO/CNTs/GCE and N-doped GO/CNTs/GCE in the potential window of 0.30 V to 0.85 V with a scanning rate of 15 mV/s into 0.1M PBS containing 60 ng/mL oxymetholone.

Figure 5 shows the outcomes of the DPV studies and the corresponding calibration plot of the N-doped GO/CNTs/GCE for each injection of the 6 ng/mL oxymetholone solution into the 0.1 M PBS (pH 7.4) solution in the potential range of 0.30 V to 0.85 V with a scanning rate of 15mV/s. According to what was discovered, the peak current intensity at 0.54 V is raised after adding 6 ng/mL oxymetholone solution to 0.1 M PBS in each DPV curve. According to the findings, N-doped GO/CNTs/GCE can capture oxymetholone molecules from the electrolyte and considerably facilitate

electron transfer [72, 73]. The calibration plot presents a linear relationship to the concentration of oxymetholone from 0 to 114ng/mL. The sensitivity is obtained at 0.18849μA/ng.mL^{-1} and the detection limit is determined as 0.01ng/mL at a signal-to-noise ratio of 3. The linear range and detection limit of the oxymetholone sensor in this work are enhanced and are better than those of the previous electrochemical reports, as shown in Table 1's summary of the electrochemical sensor's performance for determining oxymetholone in this study and other recently published oxymetholone sensors [74]. The synergistic effect of the N atoms, CNTs, and GO as signal amplification platforms for the oxidation processes of the oxymetholone molecules can be credited for the increased performance of the N-doped GO/CNTs nanocomposite.

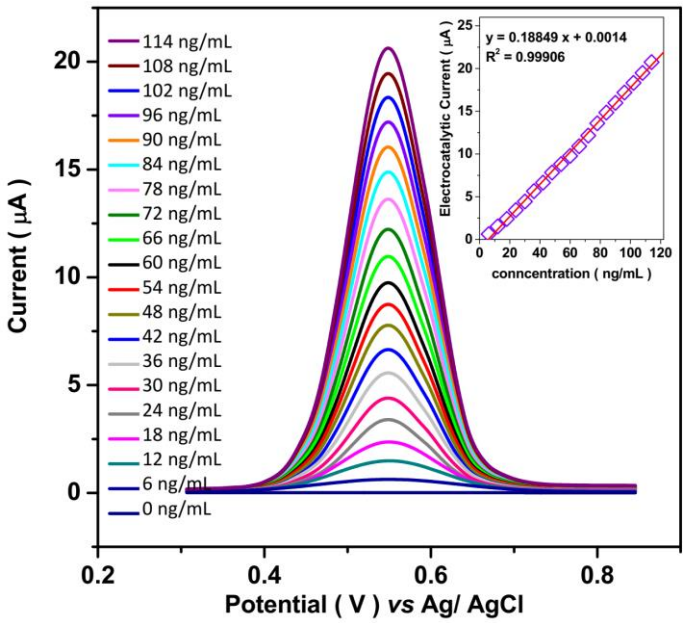

Figure 5. DPV analyses and corresponded calibration plot of N-doped GO/CNTs/GCE for each injection 6 ng/mL oxymetholone solution into 0.1 M PBS (pH 7.4) in the potential window of 0.30 V to 0.85 V with a scanning rate of 15 mV/s.

Table 1. The performance of electrochemical sensor for determination of oxymetholone in this study and other recent reported oxymetholone sensors

Electrode	Technique	LOD (ng/mL)	Linear range (ng/mL)	Ref.
N-doped GO/CNTs/GCE	DPV	0.01	0 to 114	This study
MWCNT/GCE	SWV	1.36	2.0 to 90.0	[24]
Fe_2O_3 NPs modified with sodium dodecyl sulfate	Spectrophotometry	4.0	15.0 to 3300	[21]
fused-silica capillary column	GC-MS	1	1 to 40	[22]
Hypersil ODS column	HPLC	60	120 to 600	[23]
Capillary column of LECO	GC-MS	---	0.109 to 27.324	[75]

SWV: Square wave voltammetry

Using DPV analyses with N-doped GO/CNTs/GCE at the potential window of 0.30 V to 0.85 V with a scanning rate of 15 mV/s in 0.1 M PBS (pH 7.4) under the addition of 2 ng/mL oxymetholone and 10 ng/mL of interfering species, the effect of interference on the determination of oxymetholone in human serum samples was investigated. The electrocatalytic signal results at a potential of 0.54 V are listed in Table 2, which shows that the significant electrocatalytic signal is observed after the addition of oxymetholone but not after the addition of interfering species. Therefore, it can be deduced that the proposed oxymetholone sensor demonstrates great selectivity for oxymetholone determination in clinical samples.

Table 2. Results of electrocatalytic signal at 0.54 V for N-doped GO/CNTs/GCE using DPV analysis in 0.1 M PBS (pH 7.4) under addition 2 ng/mL oxymetholone and 10 ng/mL of interfering species.

Substance	**Added (ng/mL)**	**Electrocatalytic signal (µA) at 0.54 V**	**RSD**
Oxymetholone	2	0.3770	±0.0061
Ascorbic acid	10	0.0421	±0.0017
ibuprofen	10	0.0303	±0.0021
Glucose	10	0.0205	±0.0011
propranolol	10	0.0104	±0.0015
Folic acid	10	0.0531	±0.0018
Uric acid	10	0.0402	±0.0021
azithromycin	10	0.0157	±0.0012
Acetaminophen	10	0.0100	±0.0019
amoxicillin	10	0.0361	±0.0020
Codeine	10	0.0338	±0.0017
dopamine	10	0.0195	±0.0012
Urea	10	0.0262	±0.0016
Losartan	10	0.0171	±0.0014
Fe^{2+}	10	0.0253	±0.0014
Ca^{2+}	10	0.0381	±0.0015
Na^{+}	10	0.0189	±0.0012
Mg^{2+}	10	0.0360	±0.0013

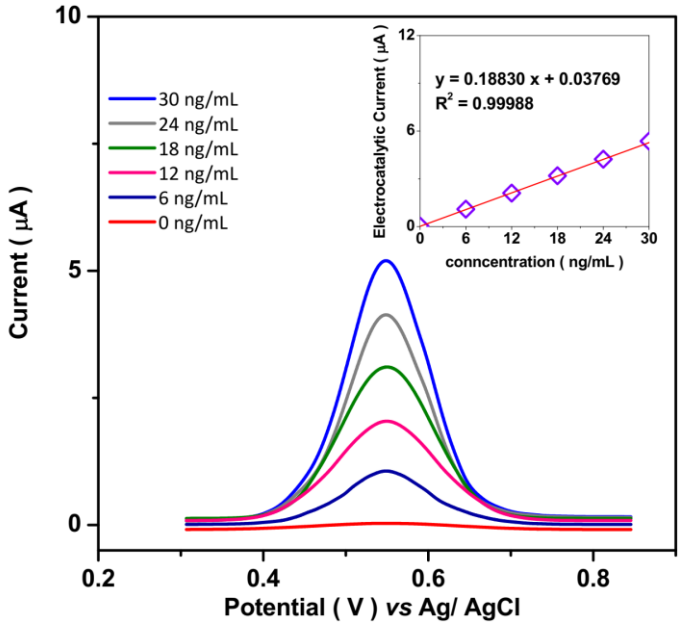

Figure 6. DPV response and calibration plot of N-doped GO/CNTs/GCE at the potential window of 0.30 V to 0.85 V with a scanning rate of 15 mV/s with serial injections of 6 ng/mL oxymetholone in 0.1 M PBS (pH 7.4) prepared from the first cyclist's blood serum sample (C1).

Table 3. The findings of DPV measurements to determination of oxymetholone in prepared real samples from cyclists's blood serum samples undergoing administration Anadrol 50

Sample No.	Detected content of oxymetholone in prepared serum samples (ng/mL)	RSD (%)
C1	0.200	±4.12
C2	0.195	±3.69
C3	0.190	±4.34
C4	0.209	±4.15

Five hours following the race, genuine blood serum samples from four riders were used to test the accuracy and usefulness of N-doped GO/CNTs/GCE for the detection of oxymetholone. The DPV response and calibration plot of N-doped GO/CNTs/GCE are shown in Figure 6 at the potential window of 0.40 V to 0.65 V with a scanning rate of 15 mV/s and serial injections of 5 µM oxymetholone in 0.1 M PBS (pH 7.4) made from the first cyclist's blood serum sample. The processed sample C1 has an oxymetholone level of 0.200 ng/mL, according to the results. The other samples (C3 to C4) were also analyzed using this method, and the findings are shown in Table 3. As seen, the detected oxymetholone levels in serum samples are close to each other. The conventional standard method was also used in the study of an actual sample C1. Table 4 displays the results of analytical studies of a prepared actual sample. As shown, the recovery (98.75 % to 99.70 %) and RSD (3.25 % to 4.15 %) values provide good precision and accuracy, indicating that this approach can be successfully employed for pharmaceutical and clinical sample evaluations.

Table 4. Findings of analytical investigations of prepared actual sample (n=3).

Spiked (ng/mL)	detected (ng/mL)	Recovery (%)	RSD (%)
0.00	0.200	----	±4.12
6.00	6.17	99.50	±3.22
12.00	12.16	99.66	±4.17
18.00	18.15	99.72	±3.15
24.00	24.12	99.66	±3.88

4. CONCULUSION

In the current study, a nanocomposite of N-doped GO and CNTs was used to fabricate an electrochemical sensor for measuring the amount of oxymetholone in blood serum samples from bikers. The N-doped GO/CNT nanocomposite was created using the pyrolysis technique, and the GCE was modified by electrochemical deposition. The corrugate sheet-like shape of the N-doped GO/CNTs nanocomposite was shown by structural analyses to contain GO nanosheets with CNTs scattered on the nanosheets. CNTs can act as a nano-spacer between GO nanosheets, essentially preventing GO nanosheet stacking. The elemental analysis showed that the N atoms were successfully inserted into the GO/CNT framework. Electrochemical studies showed that the sensitivity was obtained at 0.18849μA/ng.mL^{-1}, the detection limit was determined as 0.01ng/mL, and the calibration plot presented a linear relationship to the concentration of oxymetholone from 0 to 114ng/mL. The linear range and detection limit of the oxymetholone sensor in this work are enhanced and are better than those of recent electrochemical reports, according to a comparison of the performance of the electrochemical sensor used in this study and other recently published oxymetholone sensors. The synergistic effect of the N atoms, CNTs, and GO as signal amplification platforms for the oxidation processes of the oxymetholone molecules can be credited for the increased performance of the N-doped GO/CNTs nanocomposite. Five hours following the race, genuine blood serum samples from four riders were used to test the accuracy and usefulness of N-doped GO/CNTs/GCE for the detection of OM. The results showed that the RSD values were appropriate and acceptable for practical analyses in blood serum and clinical samples that were valid and accurate.

References

1. U.R. Hengge, K. Stocks, H. Wiehler, S. Faulkner, S. Esser, C. Lorenz, W. Jentzen, D. Hengge, M. Goos and R.E. Dudley, *Aids*, 17 (2003) 699.
2. L. Su, W. Shi, X. Chen, L. Meng, L. Yuan, X. Chen and G. Huang, *Food Chemistry*, 338 (2021) 127797.
3. H. Maleh, M. Alizadeh, F. Karimi, M. Baghayeri, L. Fu, J. Rouhi, C. Karaman, O. Karaman and R. Boukherroub, *Chemosphere*, (2021) 132928.
4. J.T. Dalton and D.D. Miller, *Nuclear Receptors as Drug Targets*, 39 (2008) 249.
5. Z. Liu, W. Su, J. Ao, M. Wang, Q. Jiang, J. He, H. Gao, S. Lei, J. Nie and X. Yan, *Nature communications*, 13 (2022) 1.

6. L. Yang, H. Huang, Z. Xi, L. Zheng, S. Xu, G. Tian, Y. Zhai, F. Guo, L. Kong and Y. Wang, *Nature communications*, 13 (2022) 1.
7. H. Li, H. Zhu and R. Zhao, *New Journal of Chemistry*, 46 (2022) 11035.
8. Y. Chen, J. Long, B. Xie, Y. Kuang, X. Chen, M. Hou, J. Gao, H. Liu, Y. He and C.-P. Wong, *ACS Applied Materials & Interfaces*, 14 (2022) 4647.
9. M. Yang, C. Li, Y. Zhang, D. Jia, X. Zhang, Y. Hou, R. Li and J. Wang, *International Journal of Machine Tools and Manufacture*, 122 (2017) 55.
10. G. Luo, J. Xie, J. Liu, Q. Zhang, Y. Luo, M. Li, W. Zhou, K. Chen, Z. Li and P. Yang, *Chemical Engineering Journal*, 451 (2022) 138549.
11. J. Dai, H. Feng, K. Shi, X. Ma, Y. Yan, L. Ye and Y. Xia, *Chemosphere*, 307 (2022) 135833.
12. I. Vahid, S. Valiollah and A. Mehdi, *Procedia-Social and Behavioral Sciences*, 1 (2009) 2843.
13. C. Zhong, H. Li, Y. Zhou, Y. Lv, J. Chen and Y. Li, *International Journal of Electrical Power & Energy Systems*, 134 (2022) 107343.
14. Y. Wang, C. Li, Y. Zhang, M. Yang, B. Li, L. Dong and J. Wang, *International Journal of Precision Engineering and Manufacturing-Green Technology*, 5 (2018) 327.
15. J. Feng, H. Gao, L. Yang, Y. Xie, A.E. El-Kenawy and A.F. El-kott, *Journal of Food Biochemistry*, 1 (2022) e14250.
16. D. Chen, Y. Li, X. Li, X. Hong, X. Fan and T. Savidge, *Chemical Science*, 13 (2022) 8193.
17. H. Karimi-Maleh, R. Darabi, M. Shabani-Nooshabadi, M. Baghayeri, F. Karimi, J. Rouhi, M. Alizadeh, O. Karaman, Y. Vasseghian and C. Karaman, *Food and Chemical Toxicology*, 162 (2022) 112907.
18. Z. Lateef Abd, *Indian Journal of Forensic Medicine & Toxicology*, 15 (2021) 3557.
19. Z. Li, M. Teng, R. Yang, F. Lin, Y. Fu, W. Lin, J. Zheng, X. Zhong, X. Chen and B. Yang, *Sensors and Actuators B: Chemical*, 361 (2022) 131691.
20. W. Yang, H. Zhang, Y. Liu, C. Tang, X. Xu and J. Liu, *RSC Advances*, 12 (2022) 14435.
21. T. Madrakian, A. Afkhami, M. Rahimi, M. Ahmadi and M. Soleimani, *Talanta*, 115 (2013) 468.
22. C.R. Cardoso, M.A.S.p. Marques, R.C. Caminha, M.C. Maioli and F.R.A. Neto, *Journal of chromatography B*, 775 (2002) 1.
23. S. Haghgoo, M. Akhavan and A.H.S. Javadi, *Research in Pharmaceutical Sciences*, 7 (2012) 632.
24. A. Afkhami, H. Ghaedi, T. Madrakian, D. Nematollahi and B. Mokhtari, *Talanta*, 121 (2014) 1.
25. Y. Pang, Q. Zhang, X. Sun, J. Ji, F. Pi and X. Shen, *International Journal of Electrochemical Science*, 13 (2018) 8518.
26. Z. Bo and T. Zhibo, *International Journal of Electrochemical Science*, 15 (2020) 6177.
27. H. Tang, T. Gao and Z. Luo, *International Journal of Electrochemical Science*, 15 (2020) 2766.
28. F. Chahshouri, H. Savaloni, E. Khani and R. Savari, *Journal of Micromechanics and Microengineering*, 30 (2020) 075001.
29. H. Karimi-Maleh, C. Karaman, O. Karaman, F. Karimi, Y. Vasseghian, L. Fu, M. Baghayeri, J. Rouhi, P. Senthil Kumar and P.-L. Show, *Journal of Nanostructure in Chemistry*, (2022) 1.
30. T.-T. Lin, W.-H. Lai, Q.-F. Lü and Y. Yu, *Electrochimica Acta*, 178 (2015) 517.
31. L. Jiang, Y. Ding, F. Jiang, L. Li and F. Mo, *Analytica chimica acta*, 833 (2014) 22.
32. L. Kong, X. Yin, X. Yuan, Y. Zhang, X. Liu, L. Cheng and L. Zhang, *Carbon*, 73 (2014) 185.
33. W. Yang, W. Liu, X. Li, J. Yan and W. He, *Journal of Advanced Research*, (2022) 1.
34. S.T. Yang, X.Y. Li, T.L. Yu, J. Wang, H. Fang, F. Nie, B. He, L. Zhao, W.M. Lü and S.S. Yan, *Advanced Functional Materials*, 32 (2022) 2202366.
35. A. Ghosh and Y.H. Lee, *ChemSusChem*, 5 (2012) 480.
36. H. Savaloni, E. Khani, R. Savari, F. Chahshouri and F. Placido, *Applied Physics A*, 127 (2021) 1.

37. Z. Savari, S. Soltanian, A. Noorbakhsh, A. Salimi, M. Najafi and P. Servati, *Sensors and Actuators B: Chemical*, 176 (2013) 335.
38. M.F.R. Hanifah, J. Jaafar, M. Othman, A. Ismail, M.A. Rahman, N. Yusof, W. Salleh and F. Aziz, *Materialia*, 6 (2019) 100344.
39. P.M. Kakade, A.R. Kachere, S.R. Rondiya and S.V. Bhosale, *ES Materials & Manufacturing*, 12 (2021) 63.
40. H. Chen and Q. Wang, *Biological Reviews*, 96 (2021) 2373.
41. B. Song, Z. Liu, L. Wang, B. Dong, D. Pan, Y. Huang, Q. Hu and Z. Guo, *Macromolecular Materials and Engineering*, 305 (2020) 2000231.
42. X. Tang, J. Wu, W. Wu, Z. Zhang, W. Zhang, Q. Zhang, W. Zhang, X. Chen and P. Li, *Analytical chemistry*, 92 (2020) 3563.
43. H. Karimi-Maleh, H. Beitollahi, P.S. Kumar, S. Tajik, P.M. Jahani, F. Karimi, C. Karaman, Y. Vasseghian, M. Baghayeri and J. Rouhi, *Food and Chemical Toxicology*, (2022) 112961.
44. Z. Wang, L. Dai, J. Yao, T. Guo, D. Hrynsphan, S. Tatsiana and J. Chen, *Bioresource Technology*, 327 (2021) 124785.
45. J. Zhang, J. Lv and J. Wang, *Zeitschrift für Kristallographie-New Crystal Structures*, 237 (2022) 385.
46. F. Zhao, L. Song, Z. Peng, J. Yang, G. Luan, C. Chu, J. Ding, S. Feng, Y. Jing and Z. Xie, *Remote Sensing*, 13 (2021) 2129.
47. F. Zhao, S. Zhang, Q. Du, J. Ding, G. Luan and Z. Xie, *Socio-Economic Planning Sciences*, 78 (2021) 101066.
48. Y. Feng, B. Zhang, Y. Liu, Z. Niu, B. Dai, Y. Fan and X. Chen, *IEEE Transactions on Microwave Theory and Techniques*, 69 (2021) 5327.
49. J. Zhang, C. Li, Y. Zhang, M. Yang, D. Jia, G. Liu, Y. Hou, R. Li, N. Zhang and Q. Wu, *Journal of cleaner production*, 193 (2018) 236.
50. X. Huang, M. Cao, D. Wang, X. Li, J. Fan and X. Li, *Optical Materials Express*, 12 (2022) 811.
51. Z. Zhu, Y. Wu and J. Han, *Frontiers in Earth Science*, (2022) 1424.
52. L. Tang, Y. Zhang, C. Li, Z. Zhou, X. Nie, Y. Chen, H. Cao, B. Liu, N. Zhang and Z. Said, *Chinese Journal of Mechanical Engineering*, 35 (2022) 1.
53. F. Yu, Z. Zhu, C. Li, W. Li, R. Liang, S. Yu, Z. Xu, F. Song, Q. Ren and Z. Zhang, *Applied Catalysis B: Environmental*, 314 (2022) 121467.
54. C. Xin, L. Changhe, D. Wenfeng, C. Yun, M. Cong, X. Xuefeng, L. Bo, W. Dazhong, H.N. Li and Y. Zhang, *Chinese Journal of Aeronautics*, (2021) 1.
55. P.-G. Ren, D.-X. Yan, X. Ji, T. Chen and Z.-M. Li, *Nanotechnology*, 22 (2010) 055705.
56. T.V. Patil, D.K. Patel, S.D. Dutta, K. Ganguly and K.-T. Lim, *Molecules*, 26 (2021) 2797.
57. Z. Zhang, C. Luo and Z. Zhao, *Natural Hazards*, 104 (2020) 2511.
58. Y. Zhao, C. Hu, Y. Hu, H. Cheng, G. Shi and L. Qu, *Angewandte Chemie International Edition*, 51 (2012) 11371.
59. R. Savari, J. Rouhi, O. Fakhar, S. Kakooei, D. Pourzadeh, O. Jahanbakhsh and S. Shojaei, *Ceramics International*, 47 (2021) 31927.
60. X. Wu, C. Li, Z. Zhou, X. Nie, Y. Chen, Y. Zhang, H. Cao, B. Liu, N. Zhang and Z. Said, *The International Journal of Advanced Manufacturing Technology*, 117 (2021) 2565.
61. L. Zhang, L. Zuo, W. Fan and T. Liu, *ChemElectroChem*, 3 (2016) 1384.
62. Y. Yang, H. Zhu, X. Xu, L. Bao, Y. Wang, H. Lin and C. Zheng, *Microporous and Mesoporous Materials*, 324 (2021) 111289.
63. T. Gao, C. Li, Y. Wang, X. Liu, Q. An, H.N. Li, Y. Zhang, H. Cao, B. Liu and D. Wang, *Composite Structures*, 286 (2022) 115232.
64. X. Li and J. Wang, *InfoMat*, 2 (2020) 3.

65. T. Li, D. Shang, S. Gao, B. Wang, H. Kong, G. Yang, W. Shu, P. Xu and G. Wei, *Biosensors*, 12 (2022) 314.
66. M. Liu, C. Li, Y. Zhang, Q. An, M. Yang, T. Gao, C. Mao, B. Liu, H. Cao and X. Xu, *Frontiers of Mechanical Engineering*, 16 (2021) 649.
67. W. Fan, Y.-E. Miao, Y. Huang, W.W. Tjiu and T. Liu, *RSC advances*, 5 (2015) 9228.
68. H. Savaloni, R. Savari and S. Abbasi, *Current Applied Physics*, 18 (2018) 869.
69. B. You, L. Wang, L. Yao and J. Yang, *Chemical communications*, 49 (2013) 5016.
70. J. Li, Y. Ma, T. Zhang, K.K. Shung and B. Zhu, *BME Frontiers*, 2022 (2022) 1.
71. X. Wang, C. Li, Y. Zhang, H.M. Ali, S. Sharma, R. Li, M. Yang, Z. Said and X. Liu, *Tribology International*, 174 (2022) 107766.
72. D. Jia, Y. Zhang, C. Li, M. Yang, T. Gao, Z. Said and S. Sharma, *Tribology International*, 169 (2022) 107461.
73. X. Cui, C. Li, Y. Zhang, Z. Said, S. Debnath, S. Sharma, H.M. Ali, M. Yang, T. Gao and R. Li, *Journal of Manufacturing Processes*, 80 (2022) 273.
74. B. Li, C. Li, Y. Zhang, Y. Wang, D. Jia and M. Yang, *Chinese Journal of Aeronautics*, 29 (2016) 1084.
75. R. Stepan, P. Cuhra and S. Barsova, *Food Additives and Contaminants*, 25 (2008) 557.